RSC Advances

PAPER

View Article Online
View Journal | View Issue

Cite this: *RSC Adv.*, 2017, **7**, 24157

Cobalt supported on Zr-modified SiO_2 as an efficient catalyst for Fischer–Tropsch synthesis

Y. J. Wu, *[abc] W. T. Zhang,[d] M. M. Yang,[b] Y. H. Zhao,[e] Z. T. Liu[a] and J. Y. Yan[c]

Amorphous silica–zirconium (SZ*x*) has been synthesized *via* the sol–gel method accompanied by phase separation in the presence of propylene oxide (PO) and poly(ethylene oxide) (PEO). Herein *x* is the mol% of zirconium (Zr), *i.e.* 0, 1.5, 2.8, 5.6 and 8.9 mol%, respectively. 13% wt% cobalt-based SZ*x* (Co/SZ*x*) catalysts were prepared by an impregnation method. The Co/SZ catalysts were characterized by XRD, N_2 adsorption–desorption, ESEM, H_2-TPR and NH_3-TPD. The catalytic behavior of Co/SZ*x* was investigated for the Fischer–Tropsch (FT) reaction *via* a fixed-bed reactor under the conditions of 1.0 MPa, $H_2/CO = 2$, $W/F = 5.05$ g h mol^{-1} and 235 °C. The results indicated that CO conversion followed the order of Co/SZ2.8 > Co/SZ1.5 > Co/SZ0 > Co/SZ5.6% > Co/SZ8.9. The activity differences for FT synthesis are mainly ascribed to the differences in SZ*x* such as Zr dosage, pore structure and aggregation extent, which are also the direct reasons for the various Co dispersions on SZ*x*. The existence of Zr in the Co/SZ catalysts leads to a decrement of the selectivity to CO_2/C_5^+, and an increase of C_2–C_4 selectivity and N-p/O value. Overall, the Co/SZ2.8 catalyst exhibited the top FT reaction activity, top yield of C_5^+ and lowest selectivity to methane and C_2–C_4 among all the Co/SZ catalysts.

Received 12th February 2017
Accepted 10th April 2017

DOI: 10.1039/c7ra01756a

rsc.li/rsc-advances

Introduction

Fischer–Tropsch synthesis (FTS) is an attractive option for the production of synthetic fuels. Much interest in FTS originates from the wide variety of carbon sources that can be used to produce synthesis gas, such as biomass, coal, or natural gas.[1,2] Additionally, the hydrocarbons produced by FTS are benign to the environment because they are free of sulfur, nitrogen, and aromatics.[3] Generally, Fe,[4] Co,[5] and Ru[6] are the active metals for FTS catalysts. However, in contrast with iron- and Ru-based catalysts, Co-based catalysts have such advantages as high activity, long service life and products with unbranched long-chain hydrocarbons found in diesel fuels.[7,8] In order to obtain a high density of metal sites (Co^0), cobalt precursors are usually dispersed on porous supports, such as amorphous SiO_2, Al_2O_3, ZrO_2, *etc.*[9–11] Among these oxides, SiO_2 is considered as inert oxide, whereas ZrO_2 and Al_2O_3 are considered as active oxides, being more interacting with the supported metals. The use of a strongly interacting oxide like alumina may increase the dispersion but decrease the reducibility. Contrarily, the use of the inert oxide like silica generally leads to a good reducibility but to an easy sintering of the Co metal. To address these problems, promoters, such as noble metal (*e.g.*, Pt, Pt,[12] Ru,[13] and Re[14]) are often used to compromise between the cobalt dispersion and reduction degree of metallic cobalt.[15] Zirconium, as a cheap promoter, has been paid attention because it may influence Co reduction, dispersion and FTS activity and selectivity. Usually, the fabrication method of zirconium-modified catalysts is impregnation, *i.e.*, as-prepared support is impregnated with Zr-included salt (*e.g.*, $ZrO(NO_3)_2$).[16–18]

To tune the metal–support interaction, in the present study, the two types of oxides, ZrO_2 and SiO_2, are combined together to form the support for FTS cobalt catalyst. ZrO_2 is added by preparation of silica–zirconium xerogel *via* sol–gel method accompanied by phase separation (SGP). Sol–gel-PS is known as a promising technique for fabricating monolithic materials with a hierarchical porous structure. This method has been used to fabricate porous SiO_2,[19] TiO_2,[20] Al_2O_3,[21] ZrO_2 [22] and mixed oxides such as Mg–Al hydrotalcite-type LDHs,[23] mullite[24] and silica–zirconia.[25]

However, few reports have been found that silica support modification by ZrO_2 prepared by SGP using ionic precursor as the zirconia source. The aim of the present investigation is (1) examine the effects of zirconium content on the properties of silica–zirconia (SZ) prepared by SGP taking zirconium oxychloride ($ZrOCl_2 \cdot 8H_2O$) and tetraethylorthosilicate (TEOS) as ZrO_2 and silica source, respectively; (2) explore the feasibility and effect mechanism of zirconium content on the catalytic activity of Co/SZ catalysts and the hydrocarbon distribution of

[a]*Key Laboratory of Applied Surface and Colloid Chemistry (MOE), School of Chemistry & Chemical Engineering, Shaanxi Normal University, Xi'an 710062, China. E-mail: yjwu76@163.com*

[b]*Department of Chemistry and Chemical Engineering, Shaanxi Xueqian Normal University, Xi'an, 710100, China*

[c]*School of Chemistry and Material Science, Hebei Normal University, Shijiazhuang, 050024, China*

[d]*Hebei Electric Power Research Institute, No. 239, Tiyu Street, Yuhua District, Shijiazhuang, 050021, China*

[e]*School of Chemistry and Environmental Engineering, Liaoning University of Technology, Jinzhou 121001, Liaoning, People's Republic of China*

FTS product. These results may provide useful information on the design of FTS catalyst.

Experimental

Preparation of silica–zirconium xerogel (SZ) and Co/SZ catalysts

Zirconium oxychloride ($ZrOCl_2 \cdot 8H_2O$) and tetraethylorthosilicate (TEOS) were used as a zirconium and silica source, respectively. A mixture of distilled water and ethanol (EtOH) was used as a solvent. Poly(ethylene oxide) (PEO; $M_v = 1 \times 10^6$) was used as a phase separation inducer. (±)-Propylene oxide (PO) was added as a proton scavenger to initiate gelation. Isopropylalcohol (IPA; 99.7%) was used to exchange the solvent of wet gels. Cobalt(II) nitrate ($Co(NO_3)_2 \cdot 6H_2O$) was used as the cobalt source. All the agents were purchased from Sinopharm Chemical Reagent Co., Ltd., China.

A series of zirconium-doped silica-based oxides in which the zirconium content was varied from 0 to 9 mol% were prepared as follows. TEOS (20 mmol), $ZrOCl_2 \cdot 8H_2O$ (0, 0.3, 0.6, 1.2 or 2.0 mmol) and PEO (50.0 mg, 5×10^{-5} mmol) were dissolved in a mixture of water (6.00 mL; 333 mmol) and ethanol (5.00 mL; 85.7 mmol). At 25 °C, PO (1.0 mL; 26.2 mmol) was added to this solution and stirred for 1 min to form a homogeneous sol. The final sol was regulated to pH 4.5 by HCl (3 mol L^{-1}) and was transferred into a polystyrene container, sealed, and kept at 60 °C to form a wet gel. The wet gel was aged for 12 h at 60 °C, subjected to solvent exchange with isopropylalcohol and then dried at 60 °C for 12 h. The resultant xerogels were subsequently heat-treated at 600 °C for 5 h with a heating rate of 2 °C min^{-1}. The obtained amorphous SZ having 0, 1.5, 3, 6 and 9 mol% of zirconium (Zr) calculated by 100 × Zr/(Zr + Si) were denoted as SZ0, 1.5, 2.8, 5.6 and 8.9 based on the results of XRF characterization, respectively.

Above SZ supports were impregnated by incipient wetness with a solution of cobalt nitrate. The final cobalt content is 13 wt% calculated by 100 × Co/(Co + SZ). Here Co and SZ are their mass, respectively. The sample was dried for 12 h and subsequently calcined at 350 °C in air for 3 h. The catalysts were denoted as Co/SZ0, Co/SZ1.5, Co/SZ2.8, Co/SZ5.6, Co/SZ8.9 according to the nomination of SZ.

Characterization of SZ and Co/SZ catalysts

The BET surface areas, pore volumes and pore size distribution were estimated from nitrogen adsorption and desorption isotherm data obtained at −196 °C using a constant-volume adsorption apparatus (Micromeritics, ASAP-2400). The pore volumes were determined at a relative pressure (P/P_o) of 0.99. The calcined samples were degassed at 300 °C under a He flow for 4 h before the measurements. The pore size distributions of the samples were determined by the BJH (Barrett–Joyner–Halenda) model from the data of desorption branch of the nitrogen isotherms.

The X-ray diffraction (XRD) patterns of SZ and Co/SZ catalysts were obtained at room temperature on a Bruker D8 Advance X-ray diffractometer using monochromatised Cu/Kα radiation (40 kV, 40 mA). The samples were scanned with a step size of 0.02° and a counting time of 0.2 s per step. The average crystallite size of Co_3O_4 was estimated by using the (311) diffraction at 2θ of about 36.8° and the Scherer's equation. The crystal size of the metallic cobalt in the reduced catalysts was calculated according to the equation of $d(Co^0) = 0.75d(Co_3O_4)$. Cobalt metal dispersion D_x(%) was calculated by using D_x (%) = $96/d(Co^0)$. The elemental analysis of SZ sample was further analyzed by using the X-ray fluorescence (XRF; SEA5120).

The morphology of the fresh SZ supports was characterized separately by using the environmental scanning electron microscope (ESEM; Quanta200, FEI, American).

Temperature programmed reduction (TPR) profiles of calcined catalysts were recorded using a Micromeritics Autochem 2920 apparatus equipped with a thermal conductivity detector (TCD). A sample (0.05 g) was pretreated by purging with flowing argon at 350 °C to remove traces of water. The TPR was performed using a 10% H_2/Ar mixture and referenced to argon at a flow rate of 30 cm^3 min^{-1}. The sample was heated from 50 to 900 °C using a heating ramp of 10 °C min^{-1}.

The temperature-programmed desorption of H_2 (H_2-TPD) and NH_3 (NH_3-TPD) were performed on a Micromeritics Autochem 2920 instrument, respectively.

For H_2-TPD, a sample (0.10 g) was reduced in pure H_2 (30 mL min^{-1}) at 400 °C for 4 h. After the system was cooled to 70 °C, Ar (30 min^{-1}) was introduced into the sample tube for 1 h to remove the physically absorbed H_2. H_2-TPD curve was then obtained by increasing the temperature from 70 °C to 410 °C at a heating rate of 10 °C min^{-1} under a He flow of 30 mL min^{-1}. Cobalt metal dispersion was calculated according to the expected 1/1 H/Co adsorption stoichiometry and the loading of cobalt.

For NH_3-TPD, a sample (0.050 g) was pretreated with Ar at 550 °C for 1 h. The sample was pretreated with 5% NH_3/He mixture for 0.5 h after it was cooled down to 120 °C and then the system was purged by pure He. Finally, NH_3-TPD was performed by increasing the temperature from 120 °C to 550 °C at a heating rate of 10 °C min^{-1} under a He flow of 30 mL min^{-1}.

FT performance of Co/SZ catalysts

Prior to activity test, the catalysts were activated in a fixed-bed reactor (I.D. = 10.0 mm) for 4 h with high-purity H_2 (50 mL min^{-1}) at 400 °C. The activity tests were conducted for around 10 h under the following reaction conditions; reaction T = 235 °C, P = 1.0 MPa, W/F = 5.0 g h mol^{-1}, feed composition (H_2/CO/Ar, mol%) = 64.11/31.90/3.99. The effluent gas from the reactor was analyzed by an online gas chromatograph (GC-9560, Shanghai Huaai) employing a HP-PONA capillary column (0.20 mm × 50 m, 0.5 μm) connected with FID for the analysis of hydrocarbons and a Porapack Q/molecular sieve (5 Å) packed column connected with TCD for the analysis of carbon oxides and Ar was selected as an internal standard gas.

Results and discussion

Texture and structure of SZ samples

Table 1 shows the weight percentages (wt%) of SiO_2 and ZrO_2 and calculated Zr mol% in SZ samples, obtained by means of

Table 1 XRF analysis of Si and Zr in SZ samples prepared in various molar ratio of $ZrOCl_2 \cdot 8H_2O$ and TEOS

Molar ratio (Si/Zr)	SiO_2 (wt%)	ZrO_2 (wt%)	Zr (mol%) from XRF (mol%)
20 : 0.0	100	0	0
20 : 0.3	97.0	3.0	1.5
20 : 0.6	94.4	5.6	2.8
20 : 1.2	89.2	10.8	5.6
20 : 2.0	83.3	16.7	8.9

XRF. All SZ samples appear a broad peak at 2θ value of 23°, which is ascribed to the characteristic diffraction of amorphous silica (Fig. 1). No obvious diffractions from ZrO_2 can be detected as the zirconium content varied from 1.5 to 8.9 mol% in SZ samples indicating that zirconium was well dispersed through the silica network.

The mesoporous structure of SZ samples has been confirmed by N_2-adsorption/desorption isotherms (Fig. 2). The sample presents type IV isotherm (definition by IUPAC)[26] which is characteristic of mesoporous material. The appearance of type H-1 hysteresis loop in the isotherm indicates the presence of uniform pores in SZ samples, which is also confirmed by the inset of Fig. 2.[27] It can be seen from Table 2 that trace ZrO_2 markedly enhances the surface area with respect to the pure sili*ca.* This indicates addition of trace ZrO_2 into SiO_2 improves the thermal stability of the pore structure both in micro- and meso-pore scales. However, the BET surface area, average pore diameter and pore volume decrease with the increasing of Zr content because Zr-rich samples are denser and more aggregation in Texture than those with low Zr content.[28]

The aggregation phenomenon can be confirmed by the ESEM images of SZ samples (Fig. 3). As shown in Fig. 3, Trace of doped zirconium (Fig. 3b and c) is favor for the stability of silica matrix. However, aggregation becomes heavier with the increasing of Zr content (Fig. 3d and e), which is unhelpful for the catalytic performance of a material.

Mixed oxides often show greatly enhanced acid activity compared with the individual component oxides due to a charge imbalance imposed upon the minor component oxide by the imposition of the bond matrix.[29] Herein SZ*x* sample is also so. As shown in Fig. 4, The TCD signal of NH_3-TPD at 140 °C and 240 °C significantly increases with the increment of Zr content from 0 to 8.9 mol% (Fig. 4), indicating Zr markedly increases the acid density of SZ mixed oxides.

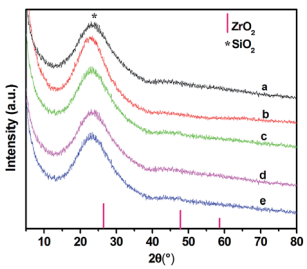

Fig. 1 XRD patterns for SZ samples (a), SZ0 (b), SZ1.5 (c), SZ2.8 (d), SZ5.6 (e), SZ8.9.

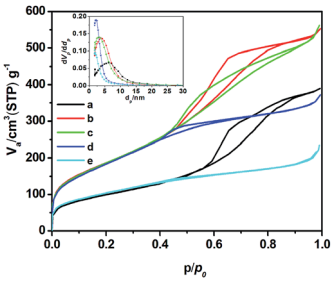

Fig. 2 Nitrogen adsorption/desorption isotherms of SZ samples (a), SZ0 (b), SZ1.5 (c), SZ2.8 (d), SZ5.6 (e), SZ8.9.

Table 2 Texture properties of SA samples

Samples	BET surface area ($m^2\ g^{-1}$)	Pore volume ($cm^3\ g^{-1}$)	Average pore diameter (nm)
SA0	357.8	0.60	6.7
SA1.5	693.5	0.88	5.2
SA2.8	686.6	0.87	5.1
SA5.6	568.1	0.54	3.8
SA8.9	372.0	0.36	3.3

Structure analysis and reduction behavior of Co/SZ*x* the catalysts

The XRD patterns of the Co/SZ*x* catalysts are given in Fig. 5. Comparing the results in Fig. 4 and 1, The new diffraction peaks at 2θ of 19.1, 31.4, 36.8, 44.9, 59.6, and 65.5° are well agreeable

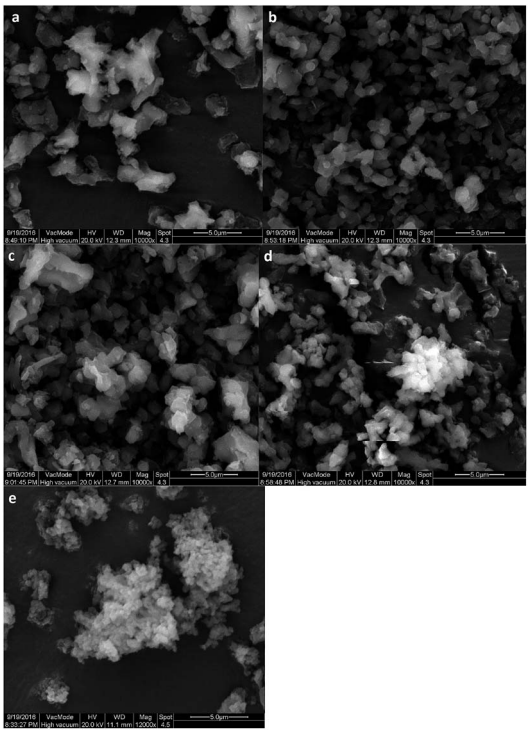

Fig. 3 ESEM images of SZ samples (a), SZ0 (b), SZ1.5 (c), SZ2.8 (d), SZ5.6 (e), SZ8.9.

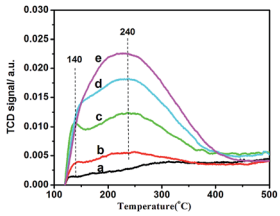

Fig. 4 NH_3-TPD profiles of SZ samples (a), SZ0 (b), SZ1.5 (c), SZ2.8 (d), SZ5.6 (e), SZ8.9.

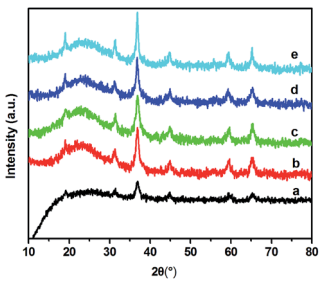

Fig. 5 XRD patterns for Co/SZ catalysts (a), Co/SZ0 (b), Co/SZ1.5 (c), Co/SZ2.8 (d), Co/SZ5.6 (e), Co/SZ8.9.

with the standard pattern of cubic Co_3O_4 (JCPDS65-3103), indicating that cobalt species over all of the calcined catalysts are primarily in the form of crystalline Co_3O_4. Moreover, the strength of the diffraction peak at 2θ of 36.8° increases with the increment of Zr content, indicating that crystallization extent of Co_3O_4 increases. This can be confirmed by the estimated sizes of Co_3O_4 based on various Zr content of Table 3. The particles size of metallic Co obtained from XRD increases from 8.0 to 11.9 nm with the increasing of Zr content from 0 to 8.9 mol%, which is well agreeable with that the results obtained H_2-TPD. The dispersion of metallic Co has a decrement tendency with the increasing of doped Zr. This may be originated from the gradually strengthened interactions between cobalt and the SZ supports due to the gradually heavier aggregation, decreased BET surface area and pore parameters of SZ samples.

The TPR patterns are displayed in Fig. 6. The reduction peak of Co/SZ1.5–8.9 corresponding to first step reduction of Co_3O_4 to CoO shows the similar temperature (270 °C) in comparison with that of Co/SZ0 catalyst. However, the reduction peak of Co/

Table 3 The crystal properties of cobalt species over different catalysts

	XRD			H_2-TPD	
Catalyst	$d(Co_3O_4)$ (nm)	$d(Co^0)$ (nm)	D_x (%)	$d(Co^0)$ (nm)	D_x (%)
Co/SZ0	10.6	8.0	12.0	7.6	7.9
Co/SZ1.5.9	12.5	9.4	10.2	9.1	7.4
Co/SZ2.8	12.7	9.5	10.1	8.7	6.9
Co/SZ5.6	13.4	10.0	9.6	9.7	6.4
Co/SZ8.9	15.9	11.9	8.1	12.1	6.0

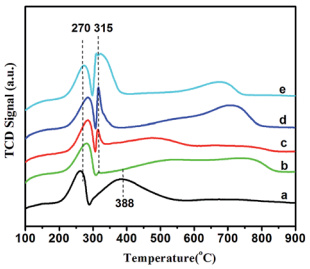

Fig. 6 H_2-TPR profiles for Co/SZ catalysts (a) Co/SZ0, (b) Co/SZ1.5, (c) Co/SZ2.8, (d) Co/SZ5.6, (e) Co/SZ8.9.

SZ1.5–8.9 corresponding to the second step reduction of CoO to Co moves to lower temperature (315 °C) in comparison with that (388 °C) of Co/SZ0 catalyst. Meanwhile, the H_2-TPR profiles of Co/SZ1.5–8.9 catalysts appear an obvious high-temperature reduction peak (>600 °C) that may be attributed to the reduction of cobalt species having strong interactions with SZ support, which is difficult to be reduced as commonly revealed.[30]

FT performance

The time-on-stream (TOS) CO conversion profiles displayed a fast increase from 1 h to 2 h followed by a slow decrease phase where CO conversion reaches a steady state at a TOS of about 6 h for all of catalysts (Fig. 7). The steady CO conversion substantially increases from 59.5% to 75.4% as Zr content is increased from 0 to 2.8 mol%, which indicates that trace Zr improve the FT activity of catalyst. This can be ascribed to the role of doped

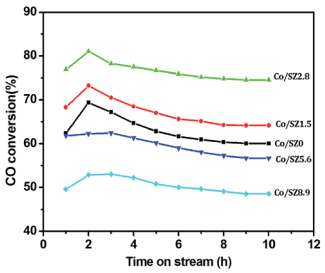

Fig. 7 The time-on-stream CO conversion of Co/SZ catalyst.

Table 4 Main results of the FT synthesis over different catalysts[a]

		Hydrocarbon distribution (%)				
Catalyst	CO_2 sel. (%)	CH_4	C_2–C_4	N-p/O[b]	C_5^+	C_5^+ yield
Co/SZ0	2.4	18.5	10.0	3.30	73.1	43.5
Co/SZ1.5	1.8	19.1	12.1	4.05	68.8	44.2
Co/SZ2.8	1.2	17.3	11.7	4.07	71.0	52.8
Co/SZ5.6	1.1	18.1	12.8	4.43	69.1	39.0
Co/SZ8.9	0.7	19.0	13.4	4.56	67.6	32.8

[a] Reaction conditions: catalyst weight = 0.5 g, T = 235 °C, P = 1.0 MPa, W/F = 5.0 g h mol^{-1}, H_2/CO = 2. [b] The molar ratio of normal paraffin to olefin in C_2–C_4 hydrocarbons.

Table 5 Catalytic performance of different FTS catalysts

Catalysts	Preparation method	CO con. (%)	CH_4 sel. (%)	C_5^+ sel. (%)	C_5^+ yield
9.4%Co–Zr/SiO_2 [16]	IWI[a]	3.0	22.0	60.0	1.8
25%Co–Zr/Al_2O_3 [18]	IWI	50.0	6.2	87.5	43.7
20%Co–Zr/SiO_2 [32]	CP[b]	45.8	14.1	75.0	34.3
13%Co–Zr/SiO_2 (here)	SGP + IWI	75.4	17.3	71.0	52.8

[a] Incipient wetness impregnation (IWI). [b] Co-precipitation (CP).

Zr that increases the pore volume (Table 2) and decreases the reduction temperature of Co_3O_4 from CoO to Co (Fig. 6), *i.e.*, exist of trivial Zr enhance the amount of the active phase (Co^0) for the Co/SZ1.5 and Co/SZ2.8 catalysts. However, as Zr content is further increased to 5.6 and 8.9 mol%, the CO conversion decreases to 56.5 and 48.6%, respectively. This may be ascribed to the heavy aggregation of SZ5.6 and 8.9 (Fig. 3), which directly lead to abbreviation of pore parameters, decrease of reduction degree for Co_3O_4 and increase of Co size.

The steady results of product distribution (TOS = 10 h) are summarized in Table 3. In comparison to the results over Co/SZ0, The CO_2 selectivity is slightly decreased and the methane selectivity has no obvious changes over Co/SZ1.5–8.9 catalysts under the same reaction conditions. This may be partly ascribed to the carbonization of methane in the presence of CO_2 expressed by eqn (1)–(4).[31]

$$\mathrm{I{-}Zr + CH_4 \rightarrow I{-}Zr{-}\overset{-}{C}H_3 + H^+} \quad (1)$$

$$\mathrm{I{-}Zr + CO_2 \rightarrow I{-}Zr{-}O{-}\overset{+}{C}{=}O} \quad (2)$$

$$\mathrm{I{-}Zr{-}\overset{-}{C}H_3 + I{-}Zr{-}O{-}\overset{+}{C}{=}O \rightarrow I{-}Zr{-}CH_3{-}\overset{O}{\overset{\|}{C}}{-}O{-}Zr{-}I} \quad (3)$$

$$\mathrm{I{-}Zr{-}CH_3{-}\overset{O}{\overset{\|}{C}}{-}O{-}Zr{-}I \xrightarrow{H_2/H^+} CH_3CH_3 + H_2O + Zr{-}I} \quad (4)$$

$$\mathrm{CH_3CH_3 \xrightarrow{\text{eqn (1)–(4)}} CH_3CH_2CH_3 \xrightarrow{\text{eqn (1)–(4)}} CH_3CH_2CH_2CH_3} \quad (5)$$

In comparison to the results over Co/SZ0, The C_2–C_4 selectivity and the value of N-p/O over Co/SZ1.5–8.9 catalysts are increased. The selectivity of C_5^+ hydrocarbons slightly decreased over Co/SZ1.5–8.9 catalysts. This may be ascribed to the synergistic effect of (1)–(5) reactions and the hydrocracking reactions of long-chain FT hydrocarbons resulted from the acidity of catalyst. Taking Co/SZ8.9 catalyst as an example, its highest amount of acidic sites (Fig. 3) *versus* the highest selectivity of C_2–C_4 and the lowest selectivity of C_5^+ hydrocarbons (Table 4) supports this explanation. Overall, Co/SZ2.8 catalyst shows the best FT activity and the top yield to C_5^+ hydrocarbons.

Comparisons of FTS properties of Co/SZ2.8 catalyst with other Zr modified FTS materials

Direct comparisons of FTS properties of Co/SZ2.8 catalyst with other Zr modified cobalt-based FTS materials are very difficult due to the different applied experimental conditions. The FTS properties of similar dosage of Zr-modified cobalt-based catalyst are summarized in Table 5.

The CO conversion and C_5^+ yield of 13%Co–Zr/SiO_2, *i.e.*, Co/SZ2.8 in this study, are the highest in the Zr-modified cobalt-based catalysts reported in the ref. 13–15 and 29 although its Co loading is only 13%. Therefore, SZ*x*, fabricated by a simple preparation process, is promising as a support used for FTS catalyst.

Conclusions

Herein amorphous SZ*x* was prepared by sol–gel route accompanied by phase separation. Co-based silica–zirconia catalysts with various mol% of zirconium content were prepared by impregnation method. SZ*x* were characterized by XRD, N_2 adsorption–desorption, ESEM, H_2-TPR and NH_3-TPD, respectively. The zirconium content in SZ*x* has a key effect on the structural and textural properties of SZ*x* and Co/SZ*x* such as the surface area, acidity, mean particle size of Co and reducibility. The surface area of SZ*x* decreases from 693.6 to 373.0 $m^2\ g^{-1}$ as zirconium content increases from 1.5% to 8.9 mol%. The mean particle size of Co from Co/SZ*x* increased from 8.0 to 11.9 nm with the changes of zirconium content from 0 to 9 mol%. The order of the catalytic behavior is Co/SZ2.8 > Co/SZ1.5 > Co/SZ0 > Co/SZ5.6 > Co/SZ8.9. The existence of zirconium has an important effect on the selectivity to the products of FTS. The doped-Zr in Co/SZ catalysts lead to the decrement of the selectivity to CO_2 and C_5^+, increase of C_2–C_4 selectivity and the increment of N-p/O. The possible mechanism is the synergistic effect of carbonization between methane and CO_2 and the hydrocracking reactions of long-chain FT hydrocarbons. On the whole, Co/SZ2.8 catalyst shows the top yield to C_5^+ and lower selectivity to methane and C_2–C_4 among the Co/SZ*x* catalysts.

Acknowledgements

This work was supported by natural science foundation of china (No. 51402324), natural science foundation of Shaanxi Province (2016JM2018) and natural science foundation of Hebei Province (B2015205172).

Notes and references

1 Q. Zhang, W. Deng and Y. Wang, *J. Energy Chem.*, 2013, **22**, 27.
2 M. E. Dry, *Catal. Today*, 2002, **71**, 227.
3 C. Knottenbelt, *Catal. Today*, 2002, **71**, 437.
4 X. B. Fan, N. Yan, Z. Y. Tao, D. E. Prof, C. X. X. Dr and K. P. Yuan, *ChemSusChem*, 2009, **2**, 941.
5 C. Chen, H. Yuuda and X. Li, *Appl. Catal., A*, 2011, **396**, 116.
6 C. X. Xiao, Z. P. Cai, T. Wang, Y. Kou and N. Yan, *Angew. Chem., Int. Ed.*, 2008, **47**(4), 746.
7 W. Ma, E. L. Kugler and D. B. Dadyburjor, *Energy Fuels*, 2007, **21**, 1832.
8 A. Y. Khodakov, W. Chu and P. Fongarland, *Chem. Rev.*, 2007, **107**, 169.
9 L. Shi, Y. Jin, C. Xing, C. Zeng, T. Kawabata, K. Imai, K. Matsuda, Y. Tan and N. Tsubaki, *Appl. Catal., A*, 2012, **435–436**, 217.
10 G. Jacobs, P. M. Patterson, Y. Zhang, T. K. Das, J. Li and B. H. Davis, *Appl. Catal., A*, 2002, **233**, 215.
11 Y. Liu, J. Chen, K. Fang, Y. Wang and Y. Sun, *Catal. Commun.*, 2007, **8**, 945.
12 A. K. Dalai and B. H. Davis, *Appl. Catal., A*, 2008, **348**, 1.
13 Y. Sun, Q. W. Sun, F. K. Jiang, J. S. Liu and Z. S. Zhang, *J. Fuel Chem. Technol.*, 2012, **40**(1), 54.
14 B. Tymowski, Y. Liu, C. Meny, C. Lefèvre, D. Begin, P. Nguyen, C. Pham, D. Edouard, F. Luck and C. Pham-Huu, *Appl. Catal., A*, 2012, **419–420**, 31.
15 H. Iida, K. Sakamoto, M. Takeuchi and A. Igarashi, *Appl. Catal., A*, 2013, **466**, 256.
16 R. J. Gregory and T. B. Alexis, *ACS Catal.*, 2016, **6**, 100.
17 X. Zhou, Q. Chen, Y. Tao and H. Weng, *Chin. J. Catal.*, 2011, **32**, 1156.
18 W. Ma, G. Jacobs, P. Gao, T. Jermwongratanachai, W. D. Shafer, V. R. R. Pendyala, C. H. Yen and L. S. J. Klettlinger, *Appl. Catal., A*, 2014, **475**, 314.
19 K. Nakanishi, *J. Porous Mater.*, 1997, **4**, 67.
20 G. Hasegawa, K. Kanamori, K. Nakanishi and T. Hanada, *J. Am. Ceram. Soc.*, 2010, **93**, 3110.
21 Y. Tokudome, K. Fujita, K. i. Nakanishi, K. Miura and K. Hirao, *Chem. Mater.*, 2007, **19**, 3393.
22 X. Guo, J. Song, Y. Lvlin, K. Nakanishi, K. Kanamori and H. Yang, *Sci. Technol. Adv. Mater.*, 2015, **16**, 25003.
23 Y. Tokudome, N. Tarutani, K. Nakanishi and M. Takahashi, *J. Mater. Chem. A*, 2013, 7702.
24 X. Guo, W. Li, K. Nakanishi, K. Kanamori, Y. Zhu and H. Yang, *J. Eur. Ceram. Soc.*, 2013, **33**, 1967.
25 R. Takahashi, S. Sato, T. Sodesawa and K. Suzuki, *J. Am. Ceram. Soc.*, 2001, **84**, 1968.
26 P. Bilyana, T. Boyko, B. Temenuzhka, P. Nartzislav, F. V. Leticia and O. A. Conchi, *Chem. Eng. J.*, 2011, **8079**, 1.
27 S. Hongbo and C. B. Elizabeth, *Chemosphere*, 2007, **68**, 1807.
28 J. A. Anderson, C. Fergusson, I. Rodrfguez-Ramos and A. Guerrero-Ruiz, *J. Catal.*, 2000, **192**, 344.
29 C. L. Thomas, *Ind. Eng. Chem.*, 1949, **41**, 2564.
30 Y. H. Zhao, Y. J. Wang, Q. Q. Hao, Z. T. Liu and Z. W. Liu, *Fuel Process. Technol.*, 2015, **136**, 87.
31 X. Wang, G. Qi, J. Xu, B. Li, C. Wang and D. Feng, *Angew. Chem., Int. Ed.*, 2012, **51**, 3850.
32 T. Miyazawa, T. Hanaoka, K. Shimura and S. Hirata, *Appl. Catal., A*, 2013, **467**, 47.